Preprint
UCRL-JC-150129

Multiphase Advection and Radiation Diffusion with Material Interfaces on Unstructured Meshes

P. Anninos

This article was submitted to
Nuclear Explosives Code Developers Conference, Monterey, California, October 20-24, 2002

October 3, 2002

U.S. Department of Energy
Lawrence Livermore National Laboratory

Multiphase advection and radiation diffusion with material interfaces on unstructured meshes

Peter Anninos
University of California
Lawrence Livermore National Laboratory, Livermore CA 94550

Abstract

A collection of numerical methods are presented for the advection or remapping of material properties on unstructured and staggered polyhedral meshes in arbitrary Lagrange-Eulerian calculations. The methods include several new procedures to track and capture sharp interface boundaries, and to partition radiation energy into multi-material thermal states. The latter is useful for extending and applying consistently single material radiation diffusion solvers to multi-material problems.

1 Basic equations

The multi-material fluid volume, mass density, momentum, and energy (hydrodynamic and radiation diffusion) continuity equations are written in a moving mesh framework as

$$\frac{\partial(JF^{[m]})}{J\,\partial t} = -\nabla_i(F^{[m]}(v^i - v_g^i)) + h^{[m]}\nabla_i v^i, \tag{1}$$

$$\frac{\partial(JF^{[m]}\rho^{[m]})}{J\,\partial t} = -\nabla_i(F^{[m]}\rho^{[m]}(v^i - v_g^i)), \tag{2}$$

$$\frac{\partial(J\rho v^k)}{J\,\partial t} = -\nabla_i(\rho v^k(v^i - v_g^i)) - \nabla_k(P + P_R), \tag{3}$$

$$\frac{\partial(JF^{[m]}\rho^{[m]}\epsilon^{[m]})}{J\,\partial t} = -\nabla_i(F^{[m]}\rho^{[m]}\epsilon^{[m]}(v^i - v_g^i)) - h^{[m]}P\nabla_i v^i + g^{[m]}c\rho(\sigma_a E - \sigma_p a_r T_e^4), \tag{4}$$

$$\frac{\partial(JE)}{J\,\partial t} = -\nabla_i(E(v^i - v_g^i)) + \nabla_i\left(\frac{c}{3\rho\sigma_r}\nabla^i E\right) - \frac{E}{3}\nabla_i v^i - c\rho\sigma_a E + c\rho\sigma_p a_r T_e^4, \tag{5}$$

where v^k is the physical velocity assumed to be the same for each material, v_g^k is the grid velocity, $\rho = \sum_m F^{[m]}\rho^{[m]}$ is the average density, $F^{[m]} = V^{[m]}/V$ is the volume fraction for material $[m]$, P is the fluid pressure, $P_R = E/3$ is the radiation pressure, $a_r(= 4a/c)$ is the radiation constant, E is the single material radiation energy, σ_r, σ_a and σ_p are the Rosseland, absorption and Planck mean opacities, T_e is the single material electron temperature, $g^{[m]}$ is a weight function for distributing radiation energy into each material, and $h^{[m]}$ is the compressibility weight coefficient. Also, J is the Jacobian of the grid geometry satisfying $\partial J/\partial t = J\nabla_i v_g^i$.

Decomposing equations (1) - (5) into their respective Lagrangian and remap parts by incorporating the convective derivative on the left-hand-side yields

$$\frac{\partial \mathbf{f}}{\partial t} + v^i\nabla_i\mathbf{f} = \mathbf{S_f} + \nabla_i(\mathbf{f}v_g^i) - \mathbf{f}\nabla_i v_g^i, \tag{6}$$

where $\mathbf{f} \equiv \{F^{[m]},\ F^{[m]}\rho^{[m]},\ \rho v^k,\ F^{[m]}\rho^{[m]}\epsilon^{[m]},\ E\}$, and $\mathbf{S_f} = \widetilde{\mathbf{S}}_\mathbf{f} - \mathbf{f}\nabla_i v^i$ with $\widetilde{\mathbf{S}}_\mathbf{f} = \partial(J\mathbf{f})/(J\partial t) + \nabla_i(\mathbf{f}(v^i - v_g^i))$ representing the right-hand-side sources without the transport terms in (1) - (5). Equation (6) is solved using operator splitting with Lagrangian $d\mathbf{f}/dt = \mathbf{S_f}$, advection $\partial\mathbf{f}/\partial t = \nabla_i(\mathbf{f}v_g^i)$, and mesh divergence $\partial\mathbf{f}/\partial t = -\mathbf{f}\nabla_i v_g^i$ parts. The following sections focus on solving the advection problem with and without material interfaces on arbitrary unstructured meshes.

2 Advection without volume fractions

When interface capturing is not needed, advection can be solved using a single step, finite volume, first order in time marching scheme, representing the discrete source term as

$$\nabla_i(\mathrm{f}v_g^i) = \frac{1}{V_Z}\int_{dV}\nabla_i(\mathrm{f}v_g^i)dV = -\frac{1}{V_Z}\oint(\mathrm{f}v_g^i)dA_i = -\frac{1}{V_Z}\sum_{F(Z)}(\mathrm{f}v_g^i)_{F(Z)}(A_i)_{F(Z)}, \tag{7}$$

where V_Z is the zone volume, and $(A_i)_{F(Z)}$ are the face area vector normals defined as the sum of the inward-pointing (towards the cell center) face-faceted area vectors of each of the tetrahedral side elements that make up the cell face, $(v_g^i)_{F(Z)}$ is the mesh velocity at the face center, and $\mathrm{f}_{F(Z)}$ is the first order extrapolated zone-centered field computed by a Taylor's expansion, $\mathrm{f}_{F(Z)} = \mathrm{f}_Z + (\nabla_i\mathrm{f})_Z^L(r^i - r_Z^i)$, from the donor cell center r_Z^i to the advection control volume center $r^i = r_{F(Z)}^i + (\Delta t/2)(v_g^i)_{F(Z)}$.

$(\nabla_i\mathrm{f})_Z^L$ is the zone-centered gradient, limited to force monotonicity in the extrapolated field variable. This is achieved by identifying three unique control volumes (assigned as upstream $\nabla_U\mathrm{f}$, downstream $\nabla_D\mathrm{f}$, or average $\nabla_A\mathrm{f}$ gradient operators) by the sign of the inner product of $\vec{A}\cdot\vec{V} \equiv (A_i)^{SF}(v_{g,N1}^i + v_{g,N2}^i)/2$, where $(A_i)^{SF}$ are the components of the face-faceted area vector of the tetrahedral side unit, and $v_{g,N1}^i$ and $v_{g,N2}^i$ are the velocity vectors at the two nodes comprising the unique edge length of the side. Each of the gradient operators are computed in a similar manner as (7) except replacing the sum over cell faces by sums over the faces in each subzonal side element that have the same sign of $\vec{A}\cdot\vec{V}$ identifying that side as contributing either to the upstream or downstream gradients. A side element is associated with the upstream (downstream) gradient if $\vec{A}\cdot\vec{V} > \delta$ ($< -\delta$), where $\delta \ll 1$. The average gradient is a composite sum of the upstream and downstream geometries, and thus includes all cell faces. The extrapolated field variables (to the face centers of the side elements) are computed as geometrically weighted averages of the zone-centered fields.

To enforce monotonicity, the reconstructed gradient $(\nabla\mathrm{f})_Z^L$ is set to zero if the inner product of any combination of the three gradient operators is less than a predetermined small number. The final gradient is limited further to various degrees of sharpness by defining the normalized scalar $\theta = \max(0,\ \nabla_i^U\mathrm{f}\nabla_A^i\mathrm{f})/\max(0,\ \nabla_i^D\mathrm{f}\nabla_A^i\mathrm{f})$, and applying either of the van Leer $\phi = (|\theta| + \theta)/(1 + |\theta|)$, or superbee limiters $\phi = \max[\min(1,\ 2\theta),\ \min(2,\ \theta)]$, to get the final expression for the zone-centered limited gradient generalized to multidimensions as

$$(\nabla\mathrm{f})_Z^L = \max(0, \nabla_i^D\mathrm{f}\nabla_A^i\mathrm{f}) \times \max(0,\ \phi) \times \frac{\nabla_A\mathrm{f}}{|\nabla_A\mathrm{f}|^2}. \tag{8}$$

A different, though somewhat more restrictive and costly, method of applying a gradient limiter on an unstructured mesh is to modify the magnitude of the average gradient operator with some parameterized function (g) of the maximum ($\nabla_{\max}$) and minimum ($\nabla_{\min}$) of the three masked gradient magnitudes

$$(\nabla_i\mathrm{f})_Z^L = \alpha\ g\,(\beta\nabla_{\max},\ (1-\beta)\nabla_{\min}) \times \frac{\nabla_A^i\mathrm{f}}{|\nabla_A^i\mathrm{f}|}. \tag{9}$$

β is a steepness parameter bounded by $0 \le \beta \le 1$, and α is a coefficient to enforce monotonicity in the extrapolated field $\mathrm{f}_{F(Z)}$: $\alpha = \min(1,\ \max(0,\ \min(\alpha_1,\ \alpha_2)))$, where $\alpha_1 = \max(0,\ \mathrm{f}_{Z+} - \mathrm{f}_Z)/(\mathrm{f}_{F(Z)} - \mathrm{f}_Z)$ if $\mathrm{f}_{F(Z)} = \mathrm{f}_Z + (\nabla_i\mathrm{f})_Z^L(r_{F(Z)}^i - r_Z^i)/\alpha > \max(\mathrm{f}_Z, \mathrm{f}_{Z+})$, or $\alpha_1 = 1$ otherwise; and $\alpha_2 = \min(0,\ \mathrm{f}_{Z+} - \mathrm{f}_Z)/(\mathrm{f}_{F(Z)} - \mathrm{f}_Z)$ if $\mathrm{f}_{F(Z)} < \min(\mathrm{f}_Z, \mathrm{f}_{Z+})$, or $\alpha_2 = 1$ otherwise. f_{Z+} refers to the field value at the opposite zone center. The min/max operations are performed over each of the faces in the zones, and α is chosen as the smallest value needed for strict monotonicity across all the faces.

3 Advection with volume fractions

Using the mass density as a template for treating general zone-centered variables, the advection equation $\partial(F^{[m]}\rho^{[m]})/\partial t = \nabla_i(F^{[m]}\rho^{[m]}v_g^i)$ is solved in the finite volume approach as

$$F^{[m],n+1/2}\rho^{[m],n+1/2} = F^{[m],n}\rho^{[m],n} - \frac{1}{V_Z^n}\sum_{F(Z)}\delta V_{F(Z)}^{[m],n}\rho_{*F(Z)}^{[m],n}\frac{v_g^i A_i}{|v_g^i A_i|}, \tag{10}$$

after the volume fraction equation $\partial F^{[m]}/\partial t = \nabla_i(v_g^i F^{[m]})$ is updated in a similar fashion. The index $n+1/2$ indicates that advection is only half the remap cycle, requiring the mesh divergence term to complete the cycle. Also, $\rho_{*F(Z)}^{[m],n}$ is the upwind value of material $[m]$ density, at time level n, upwind from face $F(Z)$, and either centered in the donor cell or extrapolated to the face or advection control volume centers using a first order monotonic expansion if the extrapolation is not performed across an interface. The remaining paragraphs in this section address the calculation of $\delta V_{F(Z)}^{[m]}$.

3.1 Interface capturing

An integral part of multi-fluid calculations is the automatic ordering of the different materials for advection with little to no user intervention. This allows for an accumulated fluid composition to be formed from materials of weighted precedence to fill the donor cell from the downstream to upstream direction (Anninos 2000). A single composite volume fraction is thus defined as $F_\downarrow^{[m]} = \min(1,\ \sum_{\ell=1}^{m} F^{[\ell]})$, where $F_\downarrow^{[m]}$ denotes the sum of volume fractions from the first m ordered materials. The advection process is repeated for each composite group of materials to compute the accumulated transfer volumes $\delta V_\downarrow^{[m]}$ across each face of the donor cell. Individual material fluxes are recovered through the normalization

$$\frac{\delta V^{[m]}}{V} = \frac{\max\left(0,\ \delta V_\downarrow^{[m]} - \sum_{\ell=1}^{m-1}\delta V^{[\ell]}\right)}{\sum_{\ell=1}^{M}\delta V^{[\ell]}}\frac{V_{acv}}{V}, \tag{11}$$

where V_{acv} is the advection control volume (formed by a face of the donor cell and the characteristics projected off the nodes of the face using the local mesh velocity), and $\delta V^{[m]}$ is the mth fluid material transfer volume bounded by the interface surface and the advection control volume.

Also, for a specified donor cell face, the corresponding upstream or opposite face cell is identified by evaluating the intersection of all other face normals with the target donor cell face. Given a fluxing face with normal $\vec{N}_0$ (defined as the sum of the constituent face-faceted side normals) and face-center position $\vec{X}_{F0}$, construct a vector originating from the face center to an arbitrarily distant position along the face normal: $\vec{X}_E = \vec{X}_{F0} + c\vec{N}_0$, where $c = c_0 V_Z/(L^{D-1})$, c_0 is a constant much greater than unity to guarantee the vector $c\vec{N}_0$ extends beyond the cell domain, L is a characteristic (minimum) cell length scale, and D is the number of space dimensions. Then loop over each of the other (j) faces in the donor cell with normals $\vec{N}^{(j)}$ and face centers $\vec{X}_F^{(j)}$, and evaluate the intersection parameter $T^{(j)} = -(X_{F0}^i N_i^{(j)} - X_F^i N_i^{(j)})/(X_E^i N_i^{(j)} - X_{F0}^i N_i^{(j)})$. The vector $\vec{X}_E - \vec{X}_{F0}$ intersects the plane $\vec{N}^{(j)}$ if $T^{(j)}$ is bounded by $0 < T^{(j)} < 1$. The upstream cell associated with a specified face is defined as the neighboring zone opposite the donor cell which shares the face with the minimum intersection parameter.

3.1.1 Aligned bisection

Many volume of fluid algorithms (DeBar 1974; Noh & Woodward 1976) assume the interface is aligned either parallel or perpendicular to the mesh. These algorithms work well if the flow geometry is primarily

aligned parallel to one coordinate direction or along the velocity vector field. However, they can become highly inaccurate for more complex geometries and flow dynamics [7].

A modified SLIC–like algorithm with improved stability and accuracy is achieved by considering five different flow topologies as determined by the volume fractions in three local (upstream, donor, and downstream) cells. The fluid distributions corresponding to the five cases are shown in Figure 1 and defined by: $F_{D-1} \leq F_c$, $F_D \geq F_c$, $F_{D+1} \geq F_c$ (Case A); $F_{D-1} \geq 1 - F_c$, $F_D \geq F_c$, $F_{D+1} \leq F_c$ (Case B); $F_{D-1} \geq F_c$, $F_D \geq F_c$, $F_{D+1} \geq F_c$ (Case C); $F_{D-1} \geq 1 - F_c$, $F_D \geq F_c$, $F_{D+1} \geq F_c$ (Case D); and $F_{D-1} \geq F_c$, $F_D \geq F_c$, $F_{D+1} \geq 1 - F_c$ (Case E). F_c is a user-specified lower bound volume fraction. The corresponding flux formulas are easily derived by integrating the bounded volume of fluid and imposing the following flux limiting constraints to account for the corner adjusted flux and locally available volume of fluid:

$$\begin{aligned}
&\text{Case A} \Rightarrow \quad \delta V = \min(F_D V,\ V_{acv} F_{D+1}),\\
&\text{Case B} \Rightarrow \quad \delta V = \min[F_D V,\ \max(0, V_{acv} - (1 - F_D)V)],\\
&\text{Case C} \Rightarrow \quad \delta V = V_{acv} F_D,\\
&\text{Case D} \Rightarrow \quad \delta V = \min[F_D V,\ V_{acv} F_{D+1} + \max((1 - F_{D+1})V_{acv} - (1 - F_D)V,\ 0)],\\
&\text{Case E} \Rightarrow \quad \delta V = \min[F_{D+1} V_{acv},\ F_D V - F_{D-1}(V - V_{acv})].
\end{aligned} \tag{12}$$

These cases are supplemented with the default $\delta V = V_{acv} F_D$ if all of (F_{D-1}, F_D, and F_{D+1}) are less than or greater than F_c, or if the volume fraction in any two adjacent cells are less than F_c.

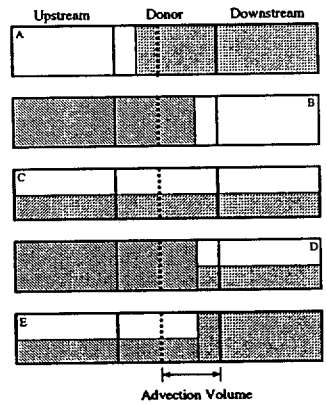

Figure 1: Different fluid volume topologies considered in the 5-rule sub-zonal grid aligned algorithm.

A second, more general, aligned bisection algorithm with improved accuracy is achieved by introducing four (six) parameters in 2D (3D) representing the dimensions of two distinct sub-zonal blocks of fluid which run the length of the donor cell along the face normals for each face of the cell. Assuming a face-normal vector pointing in the x direction, the width and height dimensions of the two fluid blocks are denoted by δx_1, δx_2, δy_1, δy_2, δz_1, and δz_2 with the block labeled with subscripts 1 (2) being more downstream (upstream) than the other. The normalized height functions are associated with volume fractions in the neighboring downstream and upstream cells

$$\delta y_1 / \Delta y = \delta z_1 / \Delta z = \sqrt{F_{D+1}}, \tag{13}$$

$$\delta y_2 / \Delta y = \delta z_2 / \Delta z = \sqrt{F_{D-1}}, \tag{14}$$

where Δy and Δz are the characteristic transverse cell dimensions, and the filling factors for each of the cross sectional areas have been assumed to be equal and related to the appropriate adjoining cell

volume fraction. The width parameters are determined by the constraints

$$\frac{\delta x_1}{\Delta x} + \frac{\delta x_2}{\Delta x} - 1 = 0, \tag{15}$$

$$\delta x_1 \delta y_1 \delta z_1 + \delta x_2 \delta y_2 \delta z_2 - F_D V_Z = 0. \tag{16}$$

The volume transfer is then defined as $\delta V / V_{acv} = F_{D+1}$ if $(V_{acv}/V_Z) \leq (\delta x_1 / \Delta x)$, or

$$\frac{\delta V}{V_{acv}} = \frac{V_Z}{V_{acv}} \frac{\delta x_1}{\Delta x} F_{D+1} + \left(1 - \frac{\delta x_1}{\Delta x} \frac{V_Z}{V_{acv}}\right) F_{D-1}, \tag{17}$$

where $\delta x_1 / \Delta x = (F_D - F_{D-1})/(F_{D+1} - F_{D-1})$ otherwise. For cases in which $\delta x_1 / \Delta x \leq 0$, the transfer volume is set to $\delta V = F_D V_{acv}$, and if $\delta x_1 / \Delta x \geq 0$, $\delta V = F_{D+1} V_{acv}$. Notice that this method does not require explicit knowledge of the precise orientation of the material interface.

3.1.2 Donor/acceptor limiter

An alternative, but slightly more computationally expensive, method to that described in §3.1.1 is the donor/acceptor concept (Hirt & Nichols 1981) based on switching between the donor or downstream cell volume fractions to flatten or steepen the fluid distribution depending on the computed interface slope. A fairly robust algorithm can be developed using minimal cell connectivity data and extended to unsplit advection. For each face, it is necessary only to estimate the interface slope (s) from local volume fraction gradients, to define a reference vector against which the interface normal is compared, to identify the appropriate donor or downstream volume fractions for each outflow cell face, and to enforce the volume fraction constraints $0 \leq F^{[i]} \leq 1$ and $0 \leq \sum_i F^{[i]} \leq 1$.

This approach uses a parameterized flux limiting formula to compute the volume of advected fluid from a downstream filling algorithm that is aligned relative to the face normal orientation. The flux limiter can be conveniently written in compact form as

$$\frac{\delta V}{V_{acv}} = \min\left[\eta + \max\left((1-\eta) - (1-\tilde{F}_D)\frac{V_Z}{V_{acv}},\ 0\right),\ \tilde{F}_D \frac{V_Z}{V_{acv}}\right], \tag{18}$$

where

$$\tilde{F}_D = F_D + \frac{1}{2}\frac{dF}{dV}(V_Z - V_{acv}), \tag{19}$$

and $\eta = F_{D+1}$ if the slope $s > s_c$ (with a critical slope s_c typically set to one or two), or $\eta = \tilde{F}_D$ otherwise. Expression (18) is derived by considering the various independent orthogonal fluid distributions in the donor and acceptor cells. The volume fraction derivative is defined as

$$\frac{dF}{dV} = \max\left(\frac{2(F_{D+1} - F_D)}{V_D + V_A},\ \frac{2(F_D - F_{D-1})}{V_D + V_U}\right), \tag{20}$$

where $V_D (\equiv V_Z)$, V_U, and V_A are the donor, upstream and acceptor cell volumes. To force a steeper boundary and help prevent the generation of floating debris, the transfer volume is redefined with $\eta = F_{D+1}$ if $F_{D+1} < F_c$, $F_D \geq F_c$ and $F_{D-1} > 1 - F_c$, or if $F_{D-1} < F_c$ and $F_D \geq F_c$.

There are many ways to estimate the slope of the interface boundary. The method used most often here associates the three-dimensional surface parameters with the local volume fraction gradients projected to each of the face normals separately. First, compute the volume fraction gradients using the most compressive (superbee) limited gradient operator defined in §2 and split the gradients into perpendicular $(\nabla_i F)^L_\perp = (\nabla_j F)^L_Z N^j_F N^i_F / N^j_F N^F_j$, and parallel $(\nabla_i F)^L_{||} = (\nabla_i F)^L_Z - (\nabla_i F)^L_\perp$, components

relative to the advecting cell face. N_F^i is a vector normal to the advecting cell face, and defined as the sum of the face-faceted area vectors of the tetrahedral side elements within the face. The interface slope is then defined as

$$s = \frac{|F_{D+1} - F_D|}{\Delta X_{AD} |(\nabla F)_{||}^L|} \max\left(0,\ \max(\ \min(1, 2\theta),\ \min(2, \theta)\ )\right), \tag{21}$$

where X_{AD} is the distance between donor and acceptor cells, and $\theta = (F_D - F_{D-1})/(F_{D+1} - F_D)$, to force monotonicity of the slope component orthogonal to the face.

3.1.3 Monotonic flux correction

These methods are similar to the donor/acceptor approach in §3.1.2 in that they use the interface slope (as defined in §3.1.2) to switch predominantly between two different fluid topologies: series or steep ($s > s_c$) versus parallel or flat ($s \leq s_c$) with $s_c = 1$ (Tipton 1994). Materials that have been grouped as series are given the highest (lowest) priority in the advection sequence if the material is dominantly downstream (upstream). The volume flux for this group of materials is computed in a grid aligned manner, and assigned as

$$\frac{\delta V}{V_{acv}} = \min\left(1,\ F_D \frac{V_Z}{V_{acv}}\right), \tag{22}$$

for leading and middle materials classified as series, or

$$\frac{\delta V}{V_{acv}} = \min\left(1,\ \max\left(0,\ 1 - (1 - F_D)\frac{V_Z}{V_{acv}}\right)\right), \tag{23}$$

for trailing materials classified as series. Fluids grouped as parallel are given intermediate priority with transfer volumes:

$$\frac{\delta V}{V_{acv}} = \min\left(1,\ \max\left(0,\ \min\left(\frac{F_D V_Z}{V_{acv}},\ \overline{F}\right)\right)\right), \tag{24}$$

where

$$\overline{F} = F_D + \frac{1}{2}(V_Z - V_{acv})\frac{dF}{dV} + cX_{AD}^i (\nabla_i F)_{||}^L, \tag{25}$$

and c is a constant to include ($c = 1$) or not ($c = 0$) the transverse interpolant using upwind discretization. The quantity dF/dV is the orthogonal (to the interface plane) volume fraction gradient computed either through (20) or by using various monotonic steepening methods. Also, the quantity $(1/2)(V_Z - V_{acv})(dF/dV)$ can be replaced by $X_{AD}^i (\nabla_i F)_{\perp}^L$ with explicit built-in monotonicity in the perpendicular gradient.

Other topological parameters, in addition to the slope, can be used to force a classification of the material distribution as either series or parallel in ambiguous situations. For example, the flow is considered as series if either $F_{D+1} < \delta$ and $F_D > 0.1$, or $F_D > (1 + \delta)F_{D-1}$, or $F_{D-1} < \delta$ and $F_{D+1} > 1 - \delta$, or $F_{D+1} < \delta$ and $F_{D-1} > 1 - \delta$, where $\delta \ll 1$. The transfer volume can also be set to $\delta V/V_{acv} = \min(1,\ F_{D+1} V_Z / V_{acv})$ if $F_{D-1} < \delta$ and $F_{D+1} > 1 - \delta$.

3.1.4 Spherical mapping

One of the more time consuming elements of piecewise linear tracking models is the problem of locating the interface (once the slope is determined) so as to match the bounded volume to the donor cell volume fraction. An approximate solution may be realized by mapping the donor grid cell onto a sphere (or

more generally an ellipsoid for anisotropic grids) with the same total volume. First consider the two–dimensional case. Letting r and r_0 represent the sphere radius and the perpendicular distance from the origin (at the center of the polygonal donor cell) to the interface boundary, the area $\widetilde{A}$ of the region bounded by the sphere and interface boundaries is given by

$$\frac{\widetilde{A}}{r^2} = \frac{\pi}{2} - \sin^{-1}\frac{r_0}{r} - \frac{r_0}{r}\sqrt{1-\left(\frac{r_0}{r}\right)^2}, \tag{26}$$

where $r = \sqrt{A/\pi}$ to match the total circular and rectangular grid cell areas (A). r_0 can be either positive for bounded areas that do not cross the origin, or negative if the bounded region includes the origin and accounts for more than half the area of the sphere. The bounded region is the domain containing the fluid and is determined by the location of the volume fraction centroid relative to the sphere center as discussed in section §3.1.5. Equation (26) is expanded out to third order in the smallness parameter $\epsilon \equiv r_0/r$

$$\frac{\widetilde{A}}{r^2} = \frac{F_D A}{r^2} \approx \frac{\pi}{2} - 2\left(\frac{r_0}{r}\right) + \frac{1}{3}\left(\frac{r_0}{r}\right)^3, \tag{27}$$

which has the real root solution directly relating r_0 to F_D

$$\frac{r_0}{r} = -(U^2+|V|)^{1/6}\left[\cos(\theta/3) - \sqrt{3}\,\sin(\theta/3)\right], \tag{28}$$

$$U = \frac{3}{2}\left(\frac{F_D A}{r^2} - \frac{\pi}{2}\right), \tag{29}$$

$$V = \left(\frac{3F_D A}{2r^2} - \frac{3\pi}{4}\right)^2 - 8, \tag{30}$$

and $\theta = \tan^{-1}(\sqrt{|V|}/U)$. Equations (28) - (30), together with the slope determined by the volume fraction gradients, uniquely defines the interface boundary without the need for iterative procedures or complex geometric modeling.

In three dimensions, the problem of computing r_0 is exact. Using the same notation for the radial parameters, the bounded fluid volume ($\widetilde{V} = F_D V$) can be expressed as

$$\frac{3\widetilde{V}}{\pi} = r_0^3 - 3r^2 r_0 + 2r^3, \tag{31}$$

with solution

$$r_0 = -(\alpha^2+\beta^2)^{1/6}\left[\cos(\theta/3) - \sqrt{3}\sin(\theta/3)\right], \tag{32}$$

$$\alpha = \frac{3F_D V}{2\pi} - r^3, \tag{33}$$

$$\beta^2 = \frac{9F_D V}{4\pi^2}\left(\frac{4\pi r^3}{3} - F_D V\right), \tag{34}$$

where $\theta = \tan^{-1}(\beta/\alpha)$ and $r = (3V/4\pi)^{1/3}$.

The plane position (or line in 2D) is then conveniently described in vector form by $\mathbf{X_p} = \mathbf{X_o} - r_0\mathbf{N}/|\mathbf{N}|$, where $\mathbf{X_o}$ is the cell center, $\mathbf{N}$ is the vector normal to the surface plane pointing away from the centroid $\mathbf{N} = -\text{sign}(\overline{\mathbf{N}}\cdot\mathbf{X^c})\,\overline{\mathbf{N}}$, and $\overline{\mathbf{N}} = (\nabla_x F, \nabla_y F, \nabla_z F)$ is the plane normal vector. Once the orientation and location of the interface surface have been determined, the volume flux bounded by the interface surface and the advection control volume is renormalized as $\delta V \rightarrow F_D V_Z \delta V / V_{IC}$, where V_{IC} is the fluid volume bounded by the interface and unclipped donor cell edges.

3.1.5 Iterative bisection

Assuming the interface slope is known, the method presented in §3.1.4 can be improved (at significant computational cost) by using a bisection procedure to repeatedly clip the cell volume with a plane until the volume bounded by the plane and cell edges on the centroid side matches the volume of fluid in the cell to a specified tolerance. The plane orientation is described by the linear form $Ax+By+Cz+D=0$, where $\overline{\mathrm{N}} = (A,\ B,\ C) = (\nabla_x F,\ \nabla_y F,\ \nabla_z F)$ is the vector normal to the plane. It is convenient to point the normal vector opposite in direction to the fluid volume centroid and, therefore, outward pointing relative to the fluid bounded by the plane. The normal vector is thus redefined as $\mathrm{N} = -\mathrm{sign}(\overline{\mathrm{N}} \cdot \mathrm{X^c})\overline{\mathrm{N}}/|\overline{\mathrm{N}}|$. The remaining parameter describing the plane position is $D = -\mathrm{N} \cdot \mathrm{X_p}$, where $\mathrm{X_p}$ is a point on the plane intersecting the normal vector running through the origin or center of the cell $\mathrm{X_o}$, $\mathrm{X_p} = \mathrm{X_o} + \lambda\ \mathrm{N}/|\mathrm{N}|$, and λ is the converging parameter of the bisection procedure representing the magnitude of the perpendicular distance of the plane to the origin. Given the plane orientation, determined by N and volume fraction gradients, and a guess position given by $\mathrm{X_p}$ (or equivalently λ), the volume of the clipped cell is computed by the following four–step process.

First, certain parameters are redefined to account for fuzzy cell boundaries. For example, to avoid difficulties arising from plane orientations which intersect the cell nodes with positions $\mathrm{X_n}$, the plane parameters are randomized for cases in which $\mathrm{N} \cdot \mathrm{X_n} + D < \delta$, where $\delta \ll 1$. Also, since the centroid plays a vital role in distinguishing the fluid side of the clipped plane, its position is redefined as $\mathrm{X^c} = \delta l \times 10^3\ \mathrm{N}$, where δl is a characteristic zone length scale, to guarantee it lies well beyond the cell boundaries and along the normal vector (but still pointing in its original sense relative to the normal). This is done in order to avoid problems when the plane is shifted along the normal vector during the bisection iterations, since $\mathrm{X_p}$ can in general lie beyond the cell boundaries.

Second, utilizing the parametric form of a straight line $\mathrm{X} = \mathrm{X_s} + t(\mathrm{X_e} - \mathrm{X_s})$, where $\mathrm{X_s}$ and $\mathrm{X_e}$ are the starting and ending positions of the line, each node on the vertices of the donor cell are checked to see of the line connecting them to the centroid intersects the clipping plane. By evaluating $t = -(D + \mathrm{X_s} \cdot \mathrm{N})/\mathrm{N} \cdot (\mathrm{X_e} - \mathrm{X_s})$, the node position (assigned to $\mathrm{X_s}$) and centroid (assigned to $\mathrm{X_e}$) lie on the same side of the clipping plane if $t < 0$ or $t > 1$. This criteria is checked for each node, and those nodes which lie on the same side of the intersecting plane as the fluid volume centroid are added to a dynamically allocated node list forming the volume boundary of the fluid.

Third, each edge connecting two nodes of the donor cell are checked to see whether it intersects the clipping plane by evaluating t with $\mathrm{X_s}$ and $\mathrm{X_e}$ representing the two nodes of the cell edge. Those edges with $0 \le t \le 1$ form an intersection with the clipping plane. The intersection point $\mathrm{X_{int}} = \mathrm{X_{n-1}} + t(\mathrm{X_n} - \mathrm{X_{n-1}})$ is added to the list of nodes forming the new face of the clipped volume.

The fourth and final step (which applies only in 3D) orders the nodes in the clipping plane intersecting the cell edges counterclockwise relative to the outward (from the fluid centroid) pointing vector. In particular, the vectors from the face center to two consecutive nodes (n and $n-1$) are ordered to satisfy $(\mathrm{X_{n-1}} - \mathrm{X_{FC}}) \times (\mathrm{X_n} - \mathrm{X_{FC}}) \cdot \mathrm{N} > 0$, where $\mathrm{X_{FC}}$ is the geometric center of the face (defined by simply averaging the node positions on the clipping plane).

4 2T Radiation diffusion with material interfaces

The coupling between radiation and hydrodynamics is achieved by assuming a constant specific heat over the solve cycle and rewriting (4), but ignoring the convective and mesh divergence terms for now, as

$$F^{[m]}\rho^{[m]}C_v^{[m]}\frac{\partial T^{[m]}}{\partial t} = -h^{[m]}P^{[m]}\nabla_i v^i + cF^{[m]}\rho^{[m]}\sigma^{[m]}(E - a_r T_e^4). \tag{35}$$

Average material quantities are constructed by defining $T = \sum F^{[m]}\rho^{[m]}C_v^{[m]}T^{[m]} / \sum F^{[m]}\rho^{[m]}C_v^{[m]}$, $C_v = \sum F^{[m]}\rho^{[m]}C_v^{[m]} / \sum F^{[m]}\rho^{[m]}$, and $\rho\sigma = \sum F^{[m]}\rho^{[m]}\sigma^{[m]}$, to approximate the single material energy equations

$$\frac{\rho C_V}{4T_e^3}\frac{\partial T_{4e}}{\partial t} = -Q_{pdv} + ca_r\rho\sigma(T_{4R} - T_{4e}), \tag{36}$$

$$\frac{\partial E}{\partial t} = \nabla_i(D\nabla^i E) - \frac{E}{3}\nabla_i v^i - c\rho\sigma(E - a_r T_{4e}), \tag{37}$$

where the notation $T_4 \equiv T^4$ is introduced for both the radiation (T_{4R}) and electron (T_{4e}) temperatures. Also, $E = a_r T_R^4$ and $Q_{pdv} = \sum_m Q_{pdv}^{[m]} = \sum_m h^{[m]}p^{[m]}\nabla_i v^i = P\nabla_i v^i$.

Two procedures are described below that can be used to easily extend single material radiation diffusion solvers to include multi-material interfaces and bridge the gap between (4) - (5) and (36) - (37). These procedures are based on formulating reasonable choices for the weight coefficient $g^{[m]}$ in equation (4), given a solution to the single material diffusion equation (37).

The first method is based on an approximate first order semi-implicit solution to the discretized multiphase internal energy equations using the time advanced solution (T_{4R}^{n+1}) to the diffusion equation

$$\frac{F^{[m]}\rho^{[m]}C_v^{[m]}}{4(T_*^{[m]})^3\Delta t}\left(T_{4e}^{[m],n+1} - T_{4e}^{[m],n}\right) = -Q_{pdv}^{[m]} + ca_r F^{[m]}\rho^{[m]}\sigma^{[m]}\left(T_{4R}^{n+1} - T_{4e}^{[m],n+1}\right). \tag{38}$$

Equation (38) is solved algebraically for $T_{4e}^{[m],n+1}$ and written as

$$T_{4e}^{[m],n+1} = \frac{F^{[m]}\rho^{[m]}C_v^{[m]}T_{*4}^{[m]} + 4(T_*^{[m]})^3(ca_r\Delta t^{[m]}F^{[m]}\rho^{[m]}\sigma^{[m]}T_{4R}^{n+1} - \Delta t\ \tilde{Q}_{pdv}^{[m]})}{F^{[m]}\rho^{[m]}C_v^{[m]} + 4ca_r\Delta t^{[m]}F^{[m]}\rho^{[m]}\sigma^{[m]}(T_*^{[m]})^3}, \tag{39}$$

with

$$\tilde{Q}_{pdv}^{[m]} = \beta F^{[m]}Q_{pdv}^{[m]} + \beta(1 - F^{[m]})\sum_j F^{[j]}Q_{pdv}^{[j]} + (1-\beta)Q_{pdv}^{[m]}, \tag{40}$$

$$T_*^{[m]} = \beta F^{[m]}T_e^{[m],n} + \beta(1 - F^{[m]})\sum_j F^{[j]}T_e^{[j],n} + (1-\beta)T_e^{[m],n}, \tag{41}$$

$$\Delta t^{[m]} = \frac{k_{CR}T_{*4}^{[m]}F^{[m]}\rho^{[m]}C_v^{[m]}}{4(T_*^{[m]})^3(\tilde{Q}_{pdv}^{[m]} + ca_r F^{[m]}\rho^{[m]}\sigma^{[m]}(T_{4R}^{n+1} - T_{*4}^{[m],n})}. \tag{42}$$

The parameter $\beta = 0$ (1) is used to neglect (include) volume fraction weighting, which makes results at extremely low volume fractions more robust and constrained to relative low scatter. Also, $T_*^{[m]}$ represents a reference temperature about which the solution is linearized, and $\Delta t^{[m]}$ is a pseudo-timestep defined with constant coefficient $k_{CR} < 1$ associated with the physical radiation Courant factor to keep temperature variations for each material relatively small.

A second procedure defines the temperature simply as a specific heat weighted average of all materials within the cell

$$T^{[m],n+1} = T^{[m],n} + \frac{\lambda^{[m]}\Delta E_R - \Delta t\ Q_{pdv}^{[m]}}{F^{[m]}\rho^{[m]}C_v^{[m]}}, \tag{43}$$

where $\Delta E_R \equiv c\rho\sigma(E - a_r T_{4e})$ is the total internal energy change due to radiation effects. Also

$$\lambda^{[m]} \equiv g^{[m]} = \begin{cases} F^{[m]}\rho^{[m]}C_v^{[m]} / \sum_j F^{[j]}\rho^{[j]}C_v^{[j]} & \text{if } \Delta E_R > 0, \\ F^{[m]}\rho^{[m]}C_v^{[m]}T^{[m]} / \sum_j F^{[j]}\rho^{[j]}C_v^{[j]}T^{[j]} & \text{otherwise,} \end{cases} \tag{44}$$

where the extra factor of $T^{[m]}$ is introduced in (44) to extract energy away predominantly from the hottest materials when the fluid is cooling ($\Delta E_R < 0$) to approximate thermal equilibrium. This approach generally yields results comparable to the previous method, though it can be less robust for very low volume fraction material, particularly when actual densities are used in place of cell average densities. Significant temperature variations can occur in both methods for materials with very small volume fractions due to the accumulation of numerical errors. In these cases, temperatures are bounded from above and below to keep variations within a specified tolerance of the mean weighted temperature.

In order to guarantee energy conservation at the end of the radiation update cycle, the material temperatures are rescaled after applying the above redistribution calculations according to

$$T_e^{[m],n+1} \rightarrow \alpha T_e^{[m],n+1} = \left(\frac{\Delta e + \sum_j F^{[j]} \rho^{[j]} C_v^{[j]} T_e^{[j],n}}{\sum_j F^{[j]} \rho^{[j]} C_v^{[j]} T_e^{[j],n+1}} \right) T_e^{[m],n+1}, \tag{45}$$

where Δe is the net (radiation + PdV summed over all materials) change in internal energy density, and the normalization factor α is constructed so that when the internal specific energy is updated by $\epsilon^{[m],n+1} = \epsilon^{[m],n} + C_v^{[m]}(T_e^{[m],n+1} - T_e^{[m],n})$, the process is conservative over the cycle such that

$$\sum_m F^{[m]} \rho^{[m]} C_v^{[m]} (T_e^{[m],n+1} - T_e^{[m],n}) = \Delta e = \Delta E_R - \Delta t \sum_m Q_{pdv}^{[m]}. \tag{46}$$

5 Comparison of interface capturing methods

Tests of the interface advection methods discussed here are versions of the classic "ball & jacks" problem: a jack of width four cells ($N_W = 4$) is superimposed within a spherical annulus of inner radius $3N_W$ and thickness N_W (in 2D), or on the exterior of a solid sphere of radius $3N_W$ (in 3D). The total length of the legs is set to $4N_W$ in 2D and $2N_W$ beyond the sphere radius in 3D.

The results presented in Figure 2 are run to a time $t = 50$ on a uniform 2D grid with 100^2 cells, unit cell widths, $v_x = v_y = 1$, and Courant factor 0.6. The images represent regions outlined by volume fraction contours $F^{[m]} = 0.7$, 0.5 and 0.3. The spherical mapping result (middle right) advects a 5–fluid system (represented by the different cross-hatched regions) to confirm the robustness of the material ordering scheme, and to verify the stability of regions where several fluids meet in a single cell. The iterative bisection solution on the bottom right assigns the slope given by the vector normal to the line joining the donor cell center and the volume fraction centroid. The other iterative bisection method (bottom left) defines the slope using Youngs (1982) weighted average procedure. Numerical accuracy is quantified from the exact 2D solutions using the average absolute error for each material over a region bounded by the radius (from the mass center) $R \leq 4N_W$. The error growth is plotted in Figure 3 as a function of time for each of the methods. Notice that the aligned bisection methods appear the most stable with the smallest absolute error and growth rate.

Figure 4 shows the end result of four 3D evolutions of the superimposed sphere and jack configuration described above. The two–fluid system undergoes rigid body rotation with a unit angular rate about an axis running through the centroid and parallel to the z direction. Results are shown after a single complete revolution on a 68^3 grid and the surface is plotted at a contour value of $F = 0.5$. Notice that the spherical mapping model and the more complex iterative method appear identical. They have in fact the same absolute error.

Acknowledgements This work was performed under the auspices of the U.S. Department of Energy by University of California, Lawrence Livermore National Laboratory under Contract W-7405-Eng-48.

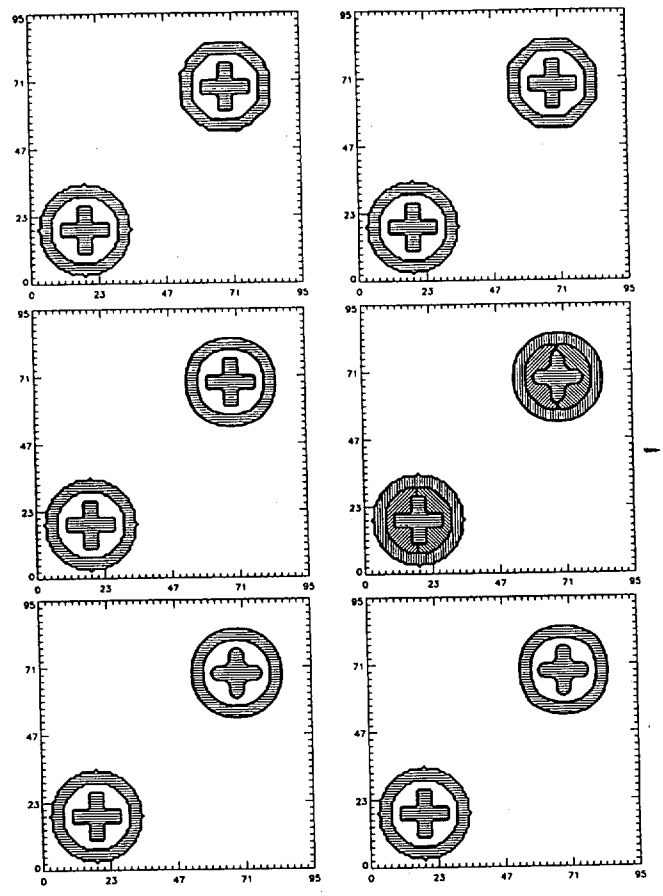

Figure 2: Results for the following interface advection methods: donor/acceptor (top left), aligned bisection (top right), monotonic flux correction (middle left), spherical mapping (middle right), iterative bisection with a Youngs-type interface slope (bottom left), iterative bisection wih a centroid-normal interface slope (bottom right).

References

[1] R. DeBar, Technical Report UCID-19683, Lawrence Livermore National Laboratory (1974)

[2] W.F. Noh and P.R. Woodward, In *Lecture Notes in Physics*; 59, A.I. van der Vooren and P.J. Zandbergen, editors, pages 330-340 (Springer-Verlag, 1976)

[3] C.W. Hirt and B.D. Nichols, *J. Comput. Phys.* **39**, 201 (1981)

[4] R. Tipton, Technical Report, Lawrence Livermore National Laboratory (1994)

[5] P. Anninos, Technical Report, Lawrence Livermore National Laboratory (2000)

[6] D.L. Youngs, In *Numerical Methods for Fluid Dynamics*, K.W. Morton and M.J. Baines, editors (Academic Press, 1982)

[7] E.G. Puckett and J.S. Saltzman, *Physica D* **60**, 84 (1992)

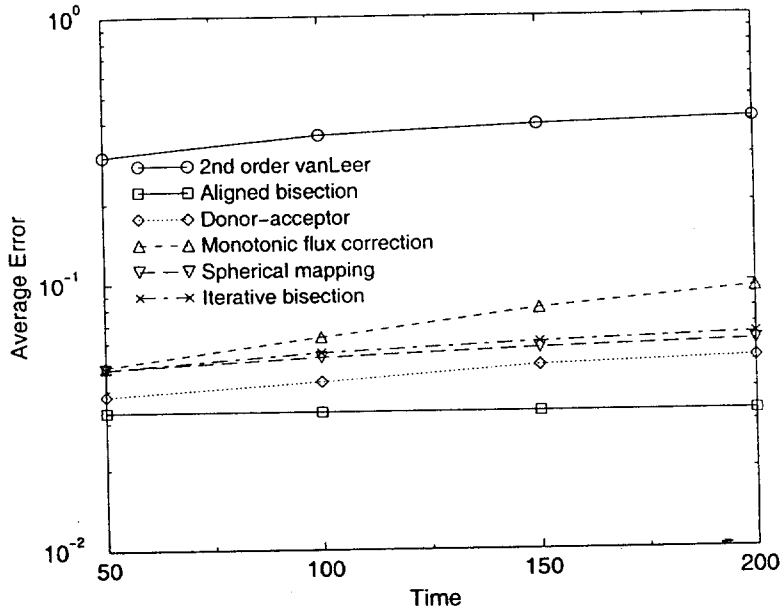

Figure 3: Comparison of numerical errors for each of the interface capturing methods discussed in this paper. Also shown for comparison are the errors for a second order van Leer advection scheme with no interface capturing.

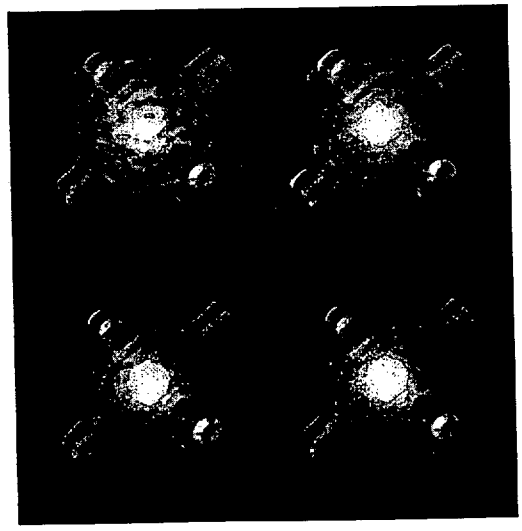

Figure 4: End results from four 3D evolutions using the following interface advection schemes: 5–rule grid aligned bisection (top left), monotonic flux correction (top right), spherical mapping (bottom left), and iterative bisection (bottom right). The results are displayed after the composite structure completed one revolution about the z–axis through the centroid.